Applied Science and Engineering Progress, Vol. 20, No. 3, 2027, 8303

Research Article

Superparamagnetic Multiphase Magnetic Activated Carbon Derived from Sugar for Rapid Methylene Blue Removal

Arie Hardian
Study Program of Master of Chemistry, Faculty of Sciences and Informatics, Universitas Jenderal Achmad Yani, Cimahi, Indonesia.
Material and Environmental Development Center, Universitas Jenderal Achmad Yani, Cimahi, Indonesia

Dani Gustaman Syarif* and Rahmawati Rahmawati
Material Responsive Radiation, Research Center for Radiation Process Technology, National Research and Innovation Agency, Serpong, Indonesia

Hakimul Wafda
Research Center for Nuclear Reactor Technology, National Research and Innovation Agency, Serpong, Indonesia

* Corresponding author. E-mail: dani001@brin.go.id DOI: 10.14416/j.asep.2026.09.004
Received: 21 May 2026; Revised: 17 July 2026; Accepted: 21 July 2026; Published online: 4 September 2026

Abstract
The development of cost-effective and easily recoverable adsorbents poses a significant challenge in wastewater treatment. This study introduces a superparamagnetic multiphase magnetic activated carbon (SM-MAC) nanocomposite, which was synthesized using a simple low-oxygen thermal method with sugar and $FeCl_2 \cdot 4H_2O$ as precursors. The carbonization was performed at 250°C for two hours, followed by activation through immersion in a sodium hydroxide solution for 48 hours, and subsequent heating at 800°C for 60 minutes in a low-oxygen atmosphere. The surface area was determined using the BET method. The crystal structure and phases were analyzed via XRD. The magnetic properties were assessed using VSM, while the functional groups of the sample were identified through FTIR. The resulting material exhibits a substantial specific surface area of 643 m^2/g, characterized by a mesoporous structure of approximately 2.7 nm, and contains various iron phases such as Fe_3O_4, Fe_2O_3, Fe_3C, and Fe, which enhance its magnetic and adsorption properties. Magnetic evaluations confirmed superparamagnetic behavior, with a saturation magnetization of 30.9 emu/g, allowing for rapid magnetic separation. The SM-MAC nanocomposite demonstrated exceptional adsorption performance for methylene blue (MB), achieving a maximum capacity between 81 and 100 mg/g and exhibiting rapid adsorption kinetics, reaching equilibrium within 15 minutes, consistent with the Langmuir isotherm models and pseudo-second-order kinetics. The SM-MAC produced shows great potential for the removal of MB.

Keywords: Adsorbent, Fe_3C, Iron oxides, Methylene blue, Superparamagnetic multiphase activated carbon

1 Introduction

The rapid growth of the global population and industrial activities has led to a substantial increase in the demand for textile and printing products. The manufacturing of these products relies heavily on synthetic dyes to achieve the desired coloration [1]-[4]. However, a significant fraction of these dyes is discharged as industrial wastewater during the production process, resulting in serious environmental pollution [1], [3], [5]. Once released into aquatic ecosystems, dye contaminants reduce water quality, inhibit light penetration, disrupt photosynthetic activity, and threaten the survival of aquatic organisms [6]-[9]. Moreover, many synthetic dyes exhibit toxic, mutagenic, or carcinogenic properties, posing considerable risks to human health through direct exposure or contaminated water resources [4], [6], [7]. Consequently, the development of efficient and sustainable technologies for dye-contaminated

Applied Science and Engineering Progress, Vol. 20, No. 3, 2027, 8303

wastewater treatment has become an increasingly important environmental challenge.

Among the various wastewater treatment technologies, photocatalytic degradation and adsorption have attracted considerable attention owing to their effectiveness in removing dye pollutants. Although photocatalysis is capable of degrading organic contaminants, its practical application is often limited by relatively low degradation efficiency under certain operating conditions, complicated synthesis procedures, and the requirement for specialized catalyst materials. In contrast, adsorption is regarded as one of the most effective and economically attractive treatment methods because of its simple operation, high removal efficiency, low energy consumption, and broad availability of adsorbent materials [10]-[14]. A wide range of natural and waste-derived resources, including biomass, minerals, and industrial by-products, has been explored as low-cost precursors for adsorbent production. Consequently, numerous adsorbent materials have been developed, such as activated carbon [15]-[17], Fe_3O_4-carbon nanocomposites [18]-[20], γ-Al_2O_3 [21], [22], Fe_3O_4 [23], [24], hydroxyapatite [12], [25], CuO [26], [27], nanosilica [8], ZnO-Al_2O_3 [28], and $CaFe_2O_4$ [29]. Despite their excellent adsorption performance, conventional adsorbents generally possess a high specific surface area that makes their separation from treated water difficult after the adsorption process. This drawback not only complicates adsorbent recovery but also limits its practical application in continuous wastewater treatment systems. To overcome this limitation, magnetic adsorbents have emerged as an attractive alternative because they can be rapidly recovered using an external magnetic field without requiring filtration or centrifugation. In particular, superparamagnetic materials have received considerable interest due to their high saturation magnetization and negligible remanent magnetization, allowing them to remain well dispersed in solution while being easily separated upon application of a magnetic field [18], [20], [29]. These characteristics improve the contact between adsorbent particles and pollutants while facilitating efficient recovery and reuse.

Among various magnetic adsorbents, magnetic activated carbon (MAC) has attracted increasing attention because it combines the high adsorption capacity of activated carbon with the convenient magnetic separation capability provided by magnetic nanoparticles. Numerous MAC-based materials have been successfully applied for the removal of organic dyes, including Congo red [30], methylene blue [10], [19], [20], crystal violet [18], and methyl orange [31], [32]. The synergistic combination of porous activated carbon and magnetic particles produces an adsorbent with high adsorption efficiency, rapid separation, and excellent reusability. Nevertheless, most reported synthesis methods involve relatively complicated procedures, such as inert gas protection, multiple synthesis steps, sophisticated equipment, and high production costs, thereby limiting their large-scale implementation. Furthermore, the influence of multiphase iron species on the adsorption mechanism and overall adsorption performance remains insufficiently understood.

In this study, we propose a simple, scalable, and cost-effective low-oxygen synthesis strategy for preparing a superparamagnetic multiphase magnetic activated carbon nanocomposite without the use of an inert atmosphere. The proposed approach significantly simplifies the synthesis process while maintaining excellent magnetic properties and adsorption performance. Furthermore, the synergistic effects of the porous carbon matrix and the incorporated multiphase iron species are systematically investigated to elucidate their respective contributions to dye adsorption and magnetic separation. The findings of this work are expected to provide valuable insights into the development of high-performance magnetic adsorbents for efficient and sustainable wastewater treatment.

2 Materials and Methods

2.1 Materials

Iron(II) chloride tetrahydrate ($FeCl_2 \cdot 4H_2O$), sodium hydroxide (NaOH), and methylene blue (MB) were acquired from Merck without any additional purification. Table sugar was provided by a mini market in Bandung.

2.2 Synthesis of superparamagnetic multiphase magnetic activated carbon (SM-MAC)

Superparamagnetic multiphase magnetic activated carbon (SM-MAC) was synthesized by mixing 16 g of sugar with 8 g of $FeCl_2 \cdot 4H_2O$ until a homogeneous precursor was obtained. The precursor was heated at 250 °C for 2 hours to obtain a carbon and iron-containing precursor. The precursor was impregnated with 1 M NaOH at a NaOH-to-precursor mass ratio of 1:1 for 48 hours, followed by filtering, washing using

aquadest until neutral pH, and drying at 100 °C for 8 h. The dried precursor was placed in an alumina crucible together with graphite powder arranged around the sample to create an oxygen-deficient environment. The crucible was covered and introduced into a muffle furnace. Carbonization was carried out by heating from room temperature to 800 °C at a rate of 10 °C min^{-1}, followed by a holding time of 1 h.

To achieve this condition, the sample was placed in a small covered alumina crucible, which was then positioned inside a larger alumina crucible filled with graphite powder, as illustrated in Figure 1. During heat treatment, the graphite powder acted as an oxygen scavenger, consuming residual oxygen and minimizing oxidation of both the carbon matrix and iron species. This simple furnace configuration enabled low-oxygen carbonization without the need for a continuous inert-gas supply, thereby promoting the formation of multiphase magnetic iron compounds. The resulting material was designated as superparamagnetic multiphase magnetic activated carbon (SM-MAC). A schematic illustration of the synthesis process is presented in Figure 2.

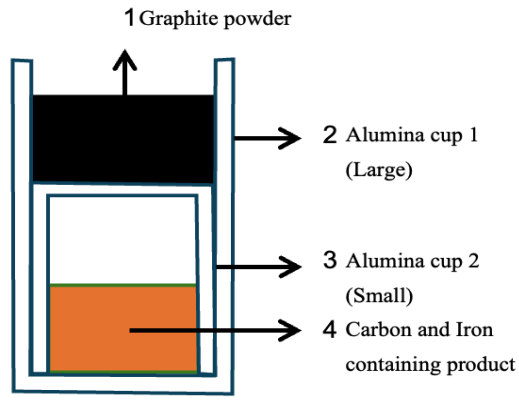

Figure 1: Heating design for composite materials used as adsorbents.

2.3 Characterization

The diffraction pattern was recorded using a diffractometer from Bruker with X-ray radiation from Cu-Kα with λ = 0.15406 nm. To find out the functional groups located on the surfaces of

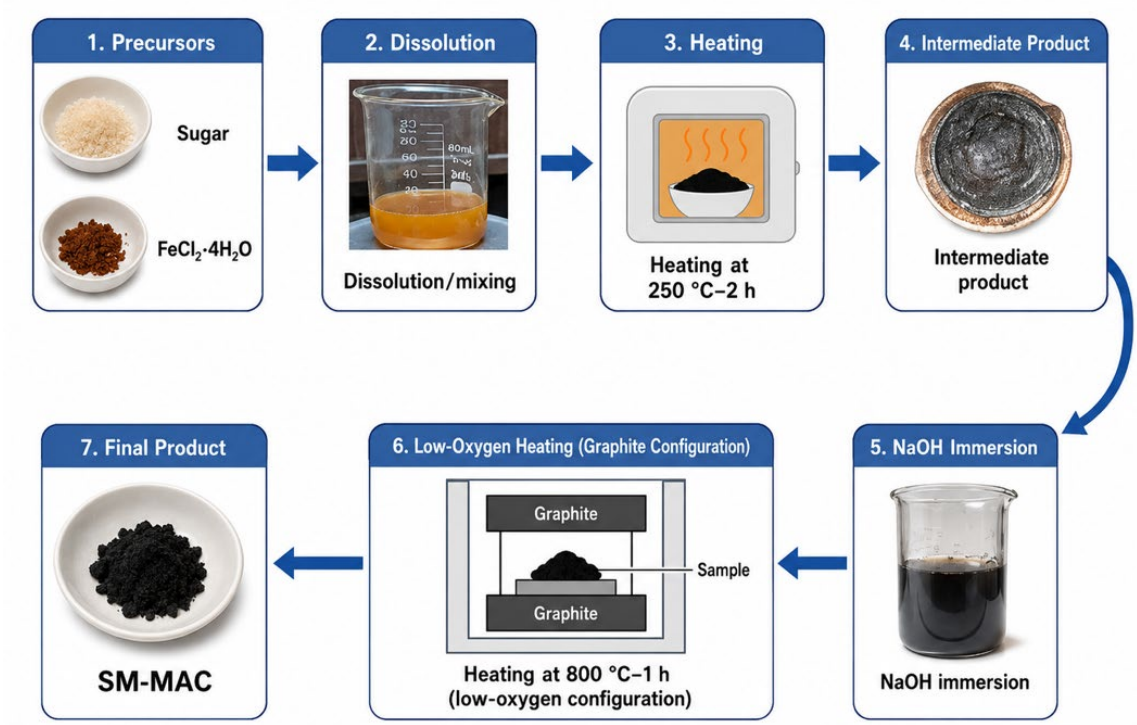

Figure 2: Schematic diagram of the MAC synthesis steps.

Applied Science and Engineering Progress, Vol. 20, No. 3, 2027, 8303

nanocomposites, the samples were examined utilizing an FTIR instrument from Thermo Scientific. To know the magnetic properties of the sample, magnetization measurements were conducted utilizing a VSM. The testing was also done by the attraction of adsorbent using an external magnet from an adsorbent containing-suspension. BET surface area and adsorbent isotherm data were measured with the aid of a surface area meter of Quantachrome.

2.4 Batch mode adsorption studies

The adsorption characteristics of methylene blue (MB), a representative pollutant present in wastewater, were analyzed by assessing the MB solution absorbance utilizing a spectrophotometer. The adsorption efficiency of the synthesized iron oxide-carbon nanocomposite was investigated at room temperature (27°C) using MB. Adsorption data were taken with two parameters: the MB solution volume and the duration of contact. A solution of MB with a concentration of 20 mg/L was prepared for this experiment. The research on adsorption kinetics and adsorption isotherm was conducted by combining 10 mg of the nanocomposite adsorbent with 20, 30, 40, 50, and 60 mL of MB at intervals of 15, 30, 45, 60, 75, 90, 105, and 120 minutes. The properties of the acquired data were examined utilizing the Langmuir as well as Freundlich equations. The pH influence on the kinetics of adsorption and isotherm was evaluated at pH values of 4.8, 7.2, and 9.1. Additionally, the starting concentration impact of the solution of MB on the efficiency of removal was examined. In each adsorption experiment, before inspection using a UV-Vis spectrometer, the adsorbent was attracted using an external magnet to the bottom of part a beaker glass. Subsequently, a few milliliters of the MB solution were extracted from the upper section of the MB solution and subjected to centrifugation for a duration of 15 minutes. The measurement of MB solution adsorption was subsequently conducted utilizing a UV-Vis spectrometer at a wavelength (λ_{max}) of 662 nm. The calculation of the dye removal efficiency (E) was carried out using equation (1) [3], [4], [6]

$$E = \frac{(C_0 - C_e)}{C_0} \times 100\% \quad (1)$$

Where, C_0 indicates the MB starting concentration, and C_e denotes the MB equilibrium concentration after adsorption. Adsorption capacity is calculated using equation (2) [4],[6].

$$Q_e = \frac{(C_0 - C_e)}{m} \times V \quad (2)$$

Where, Q_e signifies the capacity of adsorption in mg/g, C_0 represents the MB starting concentration in mg/L, C_e represents the MB equilibrium concentration after adsorption, measured in mg/L, V indicates the MB solution volume in liters (L), and m refers to the concentration of adsorbent in grams (g).

The models of adsorption isotherms and kinetics were employed to validate the mechanism of adsorption and kinetics. The models of Langmuir as well as Freundlich were employed to calculate the parameters for the MB adsorption onto the nanocomposite samples. The linearized forms of the equations of Langmuir and Freundlich are denoted by Eqs. (3) and (4) [10], [19], [29], respectively.

$$\frac{C_e}{Q_e} = \frac{1}{Q_m b} + \frac{C_e}{Q_m} \quad (3)$$

In this context, C_e indicates the MB equilibrium concentration following adsorption (mg/L), Q_e represents the adsorption capacity measured in mg/g; b the Langmuir constants; and Q_m indicates the maximum adsorption capacity, also quantified in mg/g.

$$\ln Q_e = \ln K_F + \frac{1}{n} \ln C_e \quad (4)$$

Where, C_e indicates the MB equilibrium concentration - following adsorption, quantified in mg/L, while Q_e denotes the capacity of adsorption expressed in mg/g. Additionally, K_F and n represent the constants associated with the Freundlich isotherm.

In order to explore the mechanism of adsorption kinetics, the subsequent two models were utilized: Pseudo-first-order model [5], [10], [19].

$$\ln(Q_e - Q_t) = \ln Q_e - \frac{k_1}{2.303} t \quad (5)$$

In this context, Q_e signifies the adsorption capacity quantified in mg/g, Q_t represents the adsorption capacity at a particular time t, also in mg/g, k_1 signifies the constant associated with the Pseudo-first-order model, and t refers to the time. Pseudo-second-order model [5], [10], [19].

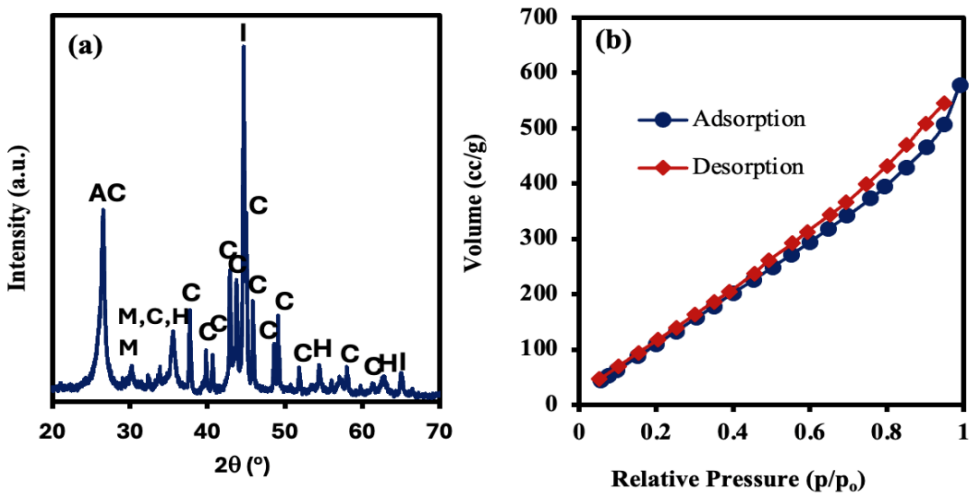

Figure 3: (a) X-ray diffraction (XRD) patterns of the synthesized SM-MAC nanocomposite, where AC is activated carbon, M is magnetit (Fe_3O_4), H is hematit (Fe_2O_3), C is cementit (Fe_3C), and I is iron (Fe) and (b) Nitrogen adsorption–desorption isotherms and pore size distribution of SM-MAC from BET analysis.

$$\frac{t}{Q_t} = \frac{1}{k_2 {Q_e}^2} + \frac{t}{Q_e} \quad (6)$$

In this context, Q_e signifies the capacity of equilibrium adsorption quantified in mg/g, whereas Q_t indicates the capacity of adsorption at a particular time t, also expressed in mg/g. The constant k_2 pertains to the Pseudo-second-order model, and t signifies time. To determine which model most accurately reflects the collected data, an evaluation of each model was conducted by analyzing the discrepancies between the calculated and experimental adsorption capacity values, along with the derived correlation coefficient R^2.

3 Results and discussion

3.1 Characterization

3.1.1 XRD analyses

The X-ray diffraction (XRD) pattern of the synthesized SM-MAC nanocomposite is presented in Figure 3a. The diffraction peaks confirm the successful formation of a multiphase magnetic nanocomposite consisting of activated carbon (AC) which aligns with the XRD pattern of activated carbon according to JCPDS (the Joint Committee on Powder Diffraction Standards) No. 36-1461, magnetite (Fe_3O_4) that is in accordance with the Fe_3O_4 XRD pattern of JCPDS No. 19-0629, hematite (Fe_2O_3) that is in accordance with the XRD pattern of Fe_2O_3 of JCPDS No. 39-1346, cementite (Fe_3C) that is in accordance with the XRD pattern of Fe_3C of JCPDS No. 35-0772, and metallic iron (Fe) that aligns with the XRD pattern of iron as specified in JCPDS No. 06-0696. The coexistence of these crystalline phases indicates that the oxygen-limited pyrolysis process not only promoted carbonization of the carbon precursor but also induced a series of reduction and carburization reactions involving the iron oxide precursor.

During thermal treatment, Fe_2O_3 initially undergoes partial reduction to Fe_3O_4 owing to the oxygen-deficient environment created by the decomposition of sugar and the evolution of reducing gases. Under prolonged heating, a fraction of Fe_3O_4 is further reduced to metallic Fe. Simultaneously, carbon generated during pyrolysis diffuses into the metallic iron particles, leading to the formation of cementite (Fe_3C). The coexistence of Fe_3O_4, Fe_2O_3, Fe_3C, and Fe therefore reflects the dynamic competition between oxidation, reduction, and carburization reactions occurring during the synthesis process. The overall transformation can be described by reactions (7-11).

At 250°C,

$$FeCl_2.2H_2O(s) + sucrose(s) \rightarrow Fe_2O_3(s) + C(s) \quad (7)$$

At 800°C under less oxygen conditions:

$$3Fe_2O_3(s) + CO(g) \rightarrow 2Fe_3O_4(s) + CO_2(g) \quad (8)$$

$$Fe_2O_3(s) + 3CO(g) \rightarrow 2Fe(s) + 3CO_2(g) \quad (9)$$

$$3Fe(s) + C(s) \rightarrow Fe_3C(s) \quad (10)$$

$$C(s) \rightarrow AC(s) \quad (11)$$

The formation of Fe_3C is particularly noteworthy because it indicates intimate contact between carbon and iron species during pyrolysis. The presence of Fe_3C is expected to contribute positively to the magnetic properties of the composite, while the coexistence of Fe_3O_4 and metallic Fe provides additional magnetic response that facilitates rapid magnetic separation (recoverability) after adsorption.

The average crystallite size of the composite components was assessed through the XRD pattern shown in Figure 3A, applying Debye Scherrer's equation (12) [5].

$$D = \frac{0.9\lambda}{\beta \cos\theta} \quad (12)$$

In this context, D denotes the particle diameter, λ is the X-ray wavelength (0.1506 nm), β signifies the full width at half maximum (FWHM), and θ indicates the diffraction angle associated with the lattice plane.

The calculated average crystallite sizes are 16.1 nm for Fe_3O_4, 28.8 nm for Fe_2O_3, 37.3 nm for Fe_3C, and 25.5 nm for metallic Fe. In addition, the average crystallite size of the activated carbon phase, estimated from the (002) reflection at $2\theta = 26.55°$, is 14.6 nm. The relatively small crystallite size of Fe_3O_4 suggests the formation of finely dispersed magnetic nanoparticles, which provide a large interfacial area between the magnetic particles and the porous carbon matrix. Such a nanostructure is advantageous because it enhances the accessibility of adsorption sites while maintaining sufficient magnetic responsiveness for efficient separation.

Furthermore, the coexistence of nanoscale magnetic phases and porous activated carbon is expected to generate a synergistic effect. The activated carbon matrix supplies abundant adsorption sites and facilitates mass transfer of dye molecules, whereas the magnetic phases enable rapid recovery of the adsorbent using an external magnetic field. This structural integration is advantageous for practical wastewater treatment because it combines high adsorption efficiency with simple and efficient post-treatment separation.

3.1.2 BET Specific Surface Area and N_2 Adsorption–Desorption Isotherms

The N_2 adsorption–desorption isotherm of the synthesized SM-MAC nanocomposite is presented in Figure 3b. According to the IUPAC classification, the adsorption isotherm exhibits a typical Type IV profile accompanied by a distinct hysteresis loop in the relative pressure (P/P_0) range of approximately 0.4–1.0, indicating the presence of a predominantly prepared by Chen *et al*. [33] and Li *et al*. [34], confirming that the synthesized material possesses a well-developed porous network suitable for adsorption applications.

Table 1: S_{BET}, pore volume, and pore diameter of carbon containing-magnetic adsorbents.

No.	Material	S_{BET} (m^2/g)	Pore volume (cm^3/g)	Pore diameter (nm)	Reference
1	PPAC-Fe_3O_4	300.1	0.2	2.21	[18]
2	Fe_3O_4@AC	1061.9	0.0206	3.6	[19]
3	Fe_3O_4.C	394.1	0.251	4.96	[31]
4	MAC	645.12	0.44	2.71	[33]
5	Fe_3O_4@C	27.65	-	17.6	[35]
6	N-PMC	290.1	0.209	-	[37]
7	ZMAC71	413.1	-	1.71	[38]
8	Fe_3O_4/C-300	56.24	0.297	20.9	[39]
9	MAC-750	359	0.37	4.11	[40]
10	MAC	643	0.892	2.77	This study

As summarized in Table 1, the synthesized SM-MAC exhibits a high specific surface area of 643 $m^2 g^{-1}$, demonstrating the effectiveness of the low-oxygen pyrolysis approach in producing highly porous magnetic activated carbon. Although Cho *et al*. [35] also synthesized magnetic activated carbon using sugar as the carbon precursor, the material prepared in the present study exhibits a considerably larger specific surface area. This improvement can be attributed to differences in the synthesis route, particularly the oxygen-limited thermal treatment, which promotes extensive carbonization and pore development while simultaneously facilitating the *in situ* formation of magnetic iron-containing phases.

The adsorption performance of porous carbon materials is strongly governed by their surface area and pore structure. A high specific surface area provides a greater number of accessible adsorption sites, thereby increasing both the adsorption capacity and the adsorption rate. In addition to surface area, pore size distribution plays a crucial role in determining the diffusion behavior of adsorbate molecules. The synthesized SM-MAC possesses an average pore diameter of 2.77 nm (Table 1), placing it within the mesoporous range defined by IUPAC (2–50 nm) [36], [39]. Mesopores are particularly advantageous for methylene blue adsorption because the effective molecular size of methylene blue is approximately 1.4 nm, allowing dye molecules to diffuse readily into the internal pore network with minimal steric hindrance. mesoporous structure. Similar adsorption behavior has been reported for magnetic activated carbon

The combination of a large specific surface area and a well-developed mesoporous architecture facilitates rapid mass transfer of methylene blue molecules from the bulk solution to the internal adsorption sites. Consequently, diffusion resistance is reduced, leading to enhanced adsorption kinetics and improved adsorption capacity. These structural characteristics are expected to contribute significantly to the superior adsorption performance of the synthesized SM-MAC compared with many previously reported magnetic carbon-based adsorbents. A comparison of the textural properties of the present material with those reported in the literature is summarized in Table 1.

3.1.2 FESEM analyses

The morphology and surface characteristics of the synthesized SM-MAC nanocomposite were investigated using field-emission scanning electron microscopy (FESEM), and the corresponding micrographs are presented in Figure 4. As shown in Figure 4a, the synthesized material exhibits two distinct morphological features: rod-shaped particles (Region 1) and porous cube-like particles (Region 2). The coexistence of these morphologies indicates the formation of a heterogeneous composite consisting of a carbon phase and an iron-containing phase, consistent with the multiphase structure identified via XRD analysis. At higher magnification (Figure 4b), the cube-like particles are observed to consist of agglomerations of spherical nanoparticles with diameters in the nanometer range. This observation aligns well with the crystallite size estimated from XRD analysis, confirming the successful formation of magnetic nanoparticles within the activated carbon matrix.

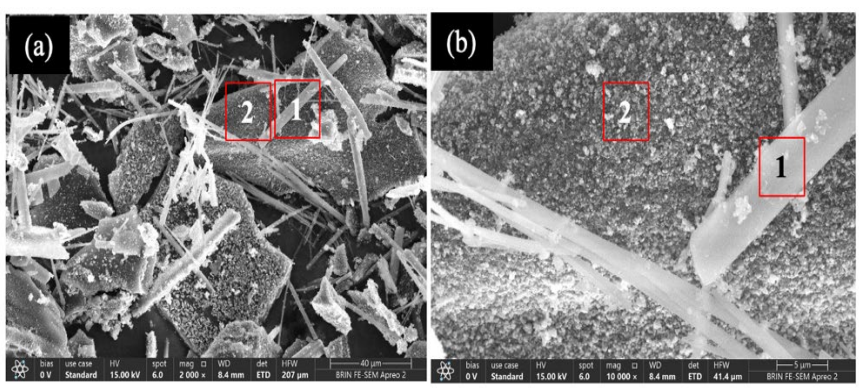

Figure 4: Field-emission scanning electron microscopy (FESEM) images of SM-MAC: (a) 2000x and (b) 10000x.

Applied Science and Engineering Progress, Vol. 20, No. 3, 2027, 8303

The porous structure observed in the FESEM images indicates that sugar decomposition during oxygen-limited pyrolysis yields a well-formed carbon network with numerous interconnected pores. The release of volatile compounds during thermal decomposition drives pore formation, while the simultaneous reduction of iron oxides triggers the *in situ* growth of magnetic nanoparticles within the carbon matrix. Consequently, the synthesized SM-MAC possesses a hierarchical architecture comprising porous activated carbon enriched with magnetic nanoparticles. The porous carbon framework provides a large, accessible surface area and abundant adsorption sites, while the nanoscale magnetic particles enhance interfacial contact between the adsorbent and dye molecules. Furthermore, the interconnected pore network facilitates the rapid diffusion of methylene blue molecules toward internal adsorption sites, thereby reducing mass transfer resistance and accelerating adsorption kinetics.

3.1.3 FTIR analyses

The FTIR spectrum of the synthesized SM-MAC nanocomposite containing activated carbon, Fe_3O_4, Fe_2O_3, Fe_3C, and metallic Fe is presented in Figure 5. The observed absorption bands confirm the successful formation of oxygen-containing functional groups on the carbon surface as well as iron oxide phases; both are believed to play a crucial role in the adsorption of methylene blue (MB). A broad absorption band centered at 3449 cm^{-1} is attributed to the stretching vibration of hydroxyl (–OH) groups, while the band at 1639 cm^{-1} corresponds to the bending vibration of adsorbed water and surface hydroxyl groups [5], [19], [33], [40]. The presence of abundant hydroxyl groups indicates that the carbon surface remains partially oxidized following pyrolysis, thereby providing hydrophilic active sites capable of interacting with dye molecules through hydrogen bonding and electrostatic interactions.

Absorption bands located at 2922 cm^{-1} and 1466 cm^{-1} are attributed to the stretching and bending vibrations of aliphatic C–H bonds, respectively [29], [40]. Meanwhile, the band observed at 1076 cm^{-1} is associated with the stretching vibration of C–O–C groups [40], which are formed during the thermal decomposition and polymerization of carbon species derived from sugar. These oxygen-containing functional groups contribute to the polarity of the adsorbent surface and enhance its affinity for cationic dye molecules.

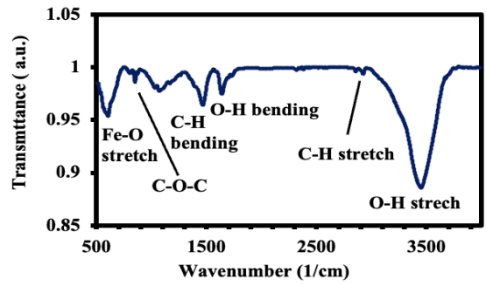

Figure 5: Fourier-transform infrared (FTIR) spectra of SM-MAC.

In the low-wavenumber region, the absorption band at 846 cm^{-1} is attributed to Fe–OH vibrations, while the strong band centered at 601 cm^{-1} corresponds to Fe–O stretching vibrations within the spinel lattice of the iron oxide nanoparticles [29]. The presence of these characteristic bands confirms the successful incorporation of the crystalline iron oxide phase into the activated carbon matrix, consistent with the XRD results. The consistency between the FTIR and XRD analyses indicates that the synthesized material consists of a carbon framework decorated with iron-containing magnetic nanoparticles.

From an adsorption perspective, the coexistence of oxygen-containing functional groups and porous carbon offers distinct advantages for methylene blue removal. The aromatic structure of the activated carbon provides graphitic domains that facilitate π–π interactions with the aromatic rings of the methylene blue molecules. Simultaneously, hydroxyl and ether groups contribute to hydrogen bonding and surface polarization, while the mesoporous carbon framework enhances the diffusion of dye molecules toward internal adsorption sites. Therefore, the adsorption of methylene blue by SM-MAC is believed to result from the synergistic contribution of π–π interactions, hydrogen bonding, electrostatic attractions, and pore-filling mechanisms, rather than a single adsorption pathway.

Furthermore, the incorporation of the iron-containing magnetic phase into the porous carbon matrix not only enables magnetic separation but also increases the structural heterogeneity of the adsorbent surface. Such heterogeneity creates adsorption sites with varying binding energies, facilitating the accommodation of dye molecules through diverse interaction mechanisms. This synergistic combination of surface chemistry, porous structure, and magnetic functionality is expected to contribute significantly to the superior adsorption performance of the synthesized SM-MAC.

3.1.4 Magnetic property analyses

The synthesized nanocomposite's magnetic properties were analyzed using a Vibrating Sample Magnetometer (VSM) at room temperature. Figure. 6a reveals the magnetization curve of the synthesized nanocomposite. This curve exhibits a sigmoidal shape with a narrow hysteresis loop, demonstrating superparamagnetic characteristics, exhibiting a saturation magnetization (Ms) of 30.9 emu/g at ambient temperature. The magnetic moment of the adsorbent examined in this study was found to be larger, smaller and comparable to that reported by other researchers, as seen in Table 2. The magnetization of the synthesized nanocomposite is sufficiently robust, allowing for easy concentration and separation from the solution by applying a magnet, as demonstrated in Figure 6b.

Table 2: Saturation magnetization (M_s) of magnetic carbonaceous sorbents.

No.	Material	M_s (emu/g)	Reference
1	MNP3	30	[31]
2	MAC	30.37	[33]
3	Fe_3O_4-C-300	23.83	[38]
4	MAC 750	8.69	[39]
5	MGO	50	[41]
6	NPG/ Fe_3O_4	46.3	[42]
7	PN-Fe_3O_4	32.74	[43]
8	Fe_3O_4-AC	20.67	[44]
9	Fe_3O_4-C	57.42	[45]
10	MAT	14.7	[46]
11	MAC	30.9	This study

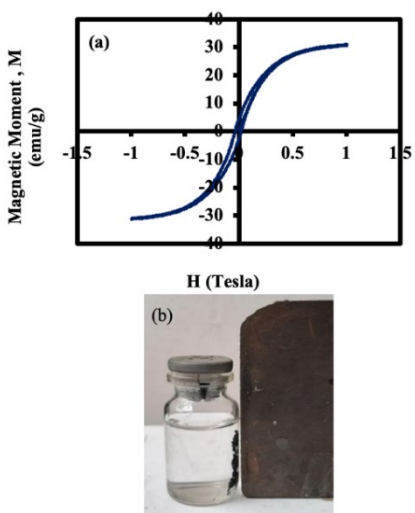

Figure 6: (a) vibrating sample magnetometry (VSM) hysteresis loop of SM-MAC, demonstrating its superparamagnetic behavior and magnetic recoverability and (b) attraction of the adsorbent by a magnet.

The adsorbent is effectively attracted by the magnet within approximately 40 seconds. The saturation magnetization of the adsorbent must reach a specific minimum value to facilitate its application. The minimum saturation magnetization for an applicable magnetic adsorbent is 16.3 emu/g [41].

The near-zero coercivity and remanence observed in the hysteresis loop confirm the superparamagnetic properties of the material, which are essential for effective magnetic recovery.

The relatively high saturation magnetization value stems from the coexistence of several magnetic phases identified via XRD, namely Fe_3O_4, Fe_3C, and metallic Fe. Magnetite acts as the primary ferrimagnetic phase, while metallic Fe contributes significantly to the overall magnetization due to its intrinsically high magnetic moment.

Additionally, cementite (Fe_3C), which is ferromagnetic at room temperature, provides an extra contribution to the composite's magnetic response. In contrast, hematite (Fe_2O_3) exhibits a much weaker magnetic response, thereby contributing minimally to the overall magnetization. The combined presence of these phases creates a synergistic magnetic effect, enabling the composite to maintain strong magnetic responsiveness despite containing a substantial amount of non-magnetic activated carbon.

3.2 Adsorption studies

The isotherm equilibrium of methylene blue (MB) on magnetic nanocomposite adsorbents as a function of equilibrium concentration for neutral pH (7.2) is illustrated in Figure 7a. The adsorption isotherm for MB is evaluated through the application of the models of Langmuir and Freundlich. The linear data from these isotherms are presented in Figures 7b and 7c. The constants obtained from the model fitting results for both Langmuir and Freundlich are summarized in Table 3. The correlation coefficient (R^2) for the fitting of the Langmuir model is 0.98, which exceeds that of the Freundlich model at 0.96. This indicates that the MB adsorption onto magnetic nanocomposite adsorbent aligns more closely with the Langmuir model, implying that the adsorption happens in a monolayer [2,3,33,40]. The maximum adsorption capacity (Q_m) obtained from the Langmuir plot for pH 7.2 is 87 mg/g.

The constants derived from fitting the Langmuir and Freundlich models for acidic pH (4.8) and basic pH (9.1) are also shown in Table 3. At a pH of 4.8,

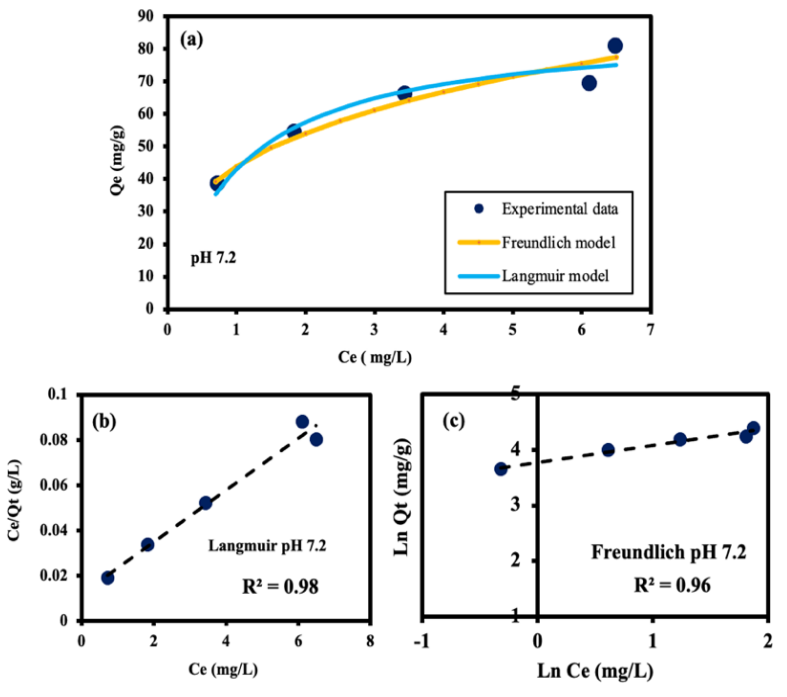

Figure 7: Equilibrium adsorption isotherms of methylene blue on SM-MAC with the corresponding Langmuir and Freundlich model fits: (a) Equilibrium isotherm with contact time 15 minutes at pH 7.2; (b) Linearized Langmuir isotherm; and (c) Linearized Freundlich isotherm.

Table 3: Fitting data of Langmuir and Freundlich models.

pH	Langmuir isotherm			Freundlich isotherm		
	Q_m (mg/g)	b (L/mg)	R^2	K_F (mg/g)(L/mg)$^{1/n}$	n	R^2
4.8	81	1	0.96	43.90	4	0.94
7.2	87	0.97	0.98	43.74	3.28	0.96
9.1	100	0.51	0.96	37.77	2.55	0.80

which represents an acidic condition, the coefficient of correlation (R^2) for the Langmuir model fit is 0.96, surpassing the value of 0.94 for the Freundlich model. Conversely, at a basic pH of 9.1, the coefficient of correlation (R^2) for the Langmuir model fit is 0.98, which is higher than the Freundlich model's coefficient of 0.80. This indicates that the MB adsorption process on magnetic nanocomposite adsorbents at pH levels of 4.8 and 9.1 aligns more closely with the Langmuir model, suggesting that the adsorption occurs in a monolayer [2],[3],[33],[40]. The maximum capacity of adsorption (Qm) derived from the Langmuir plot at pH 4.8 is 81 mg/g, while at pH 9.1 it is 100 mg/g.

In acidic conditions, the surface of the adsorbent becomes protonated. Consequently, the electrostatic repulsion among the MB cations intensifies due to this protonation. Since MB is classified as a cationic dye, the increase in electrostatic repulsion and the decrease in electrostatic attraction between the adsorbent and the molecules of MB result in a decrease in adsorption, demonstrated by a decrease in adsorption capacity.

Conversely, under basic conditions, the number of OH- ions increases, resulting in a greater negative charge on the adsorbent. This alteration strengthens the electrostatic forces between the adsorbent and MB molecules. Under these conditions, adsorption increases, which is reflected in elevated adsorption capacity. The highest adsorption capacity (Q_m) in this research for pH levels 4.8, 7.2, and 9.1 is equal to or exceeds the values reported for the adsorption of MB using magnetic carbon adsorbents, as depicted in Table 4.

Table 4: Comparative methylene blue (MB) removal (Q_m) by carbon containing-magnetic adsorbent in the last years.

No.	Material	Q_m (mg/g)	Ref.
1	Fe_3O_4 immobilized NCB	277.78	[10]
2	Fe_3O_4@AC	138.8	[19]
3	Fe_3O_4@Chili carbon	44.31	[20]
4	MAC	29.32	[32]
5	MAC	228.22	[33]
6	Fe_3O_4@C	52.63	[35]
7	MAC-750	283	[40]
8	PN-Fe_3O_4	32.5	[43]
9	Magnetized corn cob	13.23	[47]
10	Fe_3O_4-RAC	32.25	[48]
11	rGO/AK/ Fe_3O_4	39.8	[49]
12	MCM	21.27	[50]
13	MAC	81-100	This study

The kinetics of the MB adsorption using magnetic nanocomposites are illustrated in Figure 8. The uptake of MB occurs rapidly, with approximately 90.8% removal (at pH 7.2), attained in the initial 15 minutes, succeeded by a steady rise until adsorption equilibrium is achieved after 45 minutes. This rapid absorption is highly advantageous for the adsorbent. This advantage is attributed to the large specific surface area and sufficiently large the adsorbent pore volume, as supported by the data in Figure 3a and Table 1. In this study, the adsorption rate of this magnetic adsorbent is comparable to that developed by Sun et al. [17], which has been characterized as a fast-acting adsorbent. The adsorbent performs better in a basic environment (uptake around 91.7% at pH 9.1) and is less effective in an acidic environment (uptake about 89% at pH 4.8) as clearly demonstrated

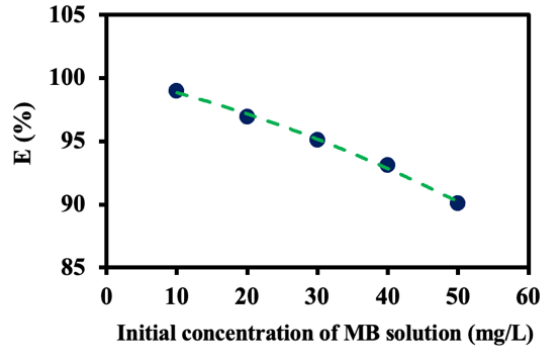

Figure 8: Removal efficiency as a function of the initial concentration of MB solution.

also in the research conducted by Misran et al. [4] and Aryee et al. [43].

The kinetics of adsorption were assessed to ascertain if they conform to the pseudo-first-order or pseudo-second-order model (Table 5). At a neutral pH of 7.2, as illustrated in Figure 7c (Pseudo-first- order) and Figure 7d (pseudo-second-order), it is clear that the correlation coefficient for the Pseudo-second-order model (1) exceeds that of the pseudo-first-order model (0.82). This information suggests that at a pH of 7.2, the process of adsorption follows the model of Pseudo- second-order. This implies that the dominant adsorption mechanism is a chemical process (Chemisorption) [3], [32], [40]. Furthermore, for the acidic and basic pH of 4.8 and 9.1, the coefficient of correlation for the model of Pseudo-second-order and that of the model of Pseudo-first-order are shown in Table 5. It is evident that the correlation coefficient for the model of Pseudo-second-order at pH 4.8 and 9.1 surpasses that of the Pseudo-first-order model. This information suggests that the process of adsorption at mechanism of adsorption is chemical in nature (Chemisorption) [3], [32], [40].

It is plausible that the partial charges of superparamagnetic multiphase magnetic

Table 5: Kinetic parameter calculated from pseudo-first and second order models.

Model	Kinetic parameter	pH		
		4.8	7.2	9.1
Pseudo-first-order	K_1 (min^{-1})	0.17	0.16	0.21
	R^2	0.85	0.82	0.77
	Qe ($mg \cdot g^{-1}$)	22.14	14.63	18.01
Pseudo-second-order	K_2 ($g \cdot mg^{-1} \cdot min^{-1}$)	0.015	0.025	0.027
	R^2	1	1	1
	Qe ($mg \cdot g^{-1}$)	57.14	57.14	57.47

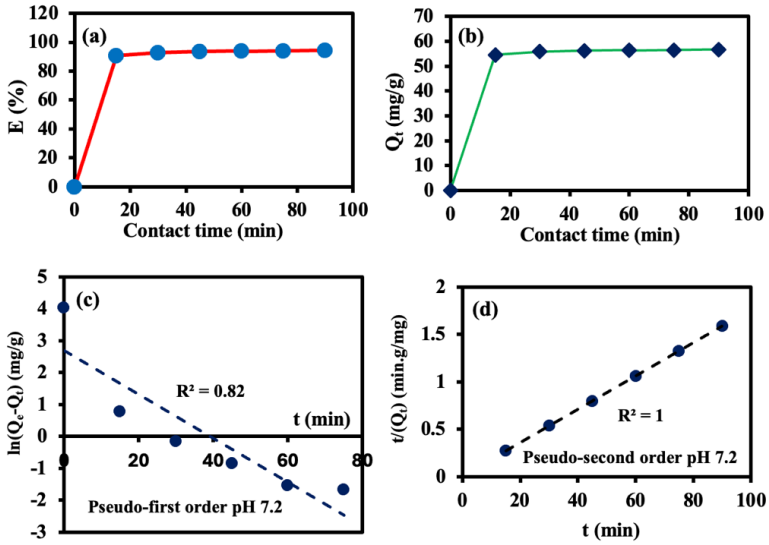

Figure 9: Adsorption kinetics of methylene blue onto SM-MAC under the investigated experimental conditions: (a) efficiency; (b) Adsorption as a function of time for a 30 mL (20 mg/L) MB solution at pH 7.2; (c) Pseudo-first-order kinetics; and (d) Pseudo-second-order kinetics.

nanocomposite adsorbent (SM-MAC) containing Fe_3O_4, Fe_2O_3, Fe_3C, and Fe interact with the MB molecules. According to the FTIR spectra, carboxyl and hydroxyl functional groups found on the magnetic nanocomposite have the ability to electrostatically attract cationic MB. Furthermore, an additional potential that contributes to the MB adsorption is the complexation that takes place during the process of adsorption involving MB and iron-based materials. The Fe-O group existence in the spectrum of FTIR corroborates this process. Additionally, the size of the nanocomposite significantly influences the degradation process, as smaller particle sizes create a pH 4.8 and 9.1 also conforms to the model of Pseudo-second-order. This implies that the primary greater potential difference between nanocomposite and MB, resulting in enhanced catalytic activity. These findings indicate that the pseudo-second-order model effectively characterizes the methylene blue (MB) adsorption kinetics onto the magnetic nanocomposite adsorbent. According to the findings derived from the model of pseudo-second-order, the rate-limiting step in the adsorption process is ascribed to chemisorption [3],[32],[40]. This process involves the sharing or exchange of electrons between the adsorbent and the MB dye.

The impact of the initial concentration of MB solution on the efficiency of removal (E) for a contact time of 45 minutes is illustrated in Figure 8. As indicated in Figure 8, the removal efficiency diminishes from 99 % to 90 % subsequent to the rise in the MB solution concentration from 10 mg/L to 50 mg/L. This phenomenon arises from the enhancement of the adsorbent surface charge, which subsequently diminishes the dye removal effectiveness [19].

3.2.1 Reusability evaluation

The reusability of the SM-MAC adsorbent was assessed by conducting adsorption measurements adsorbent was conducted using 96% ethanol. Reusability across cycles exhibited a gradual reduction in adsorption efficiencies over the course of five cycles, with the removal of MB decreasing from 99% to 86% (Figure 10).

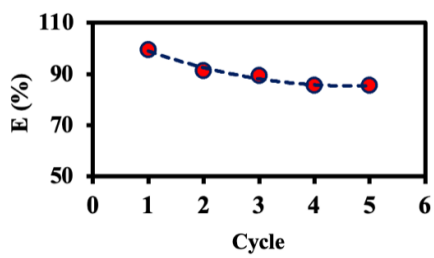

Figure 10: The efficiency of adsorption as a function of the cycle.

This gradual decline in removal efficiency (E) after repeated adsorption-desorption cycles indicates a partial loss of active sites, likely due to fouling and incomplete desorption [51],[52]. This information aligns with a study that reported a decrease in efficiency with repeated cycles [52]. According to that study, adsorbents exhibiting such a reduction in removal efficiency still possess practical reusability capabilities [52].

3.2.2 Adsorption Mechanism

Based on the combined results of XRD, BET, FESEM, and FTIR analyses, along with magnetic characterization, adsorption kinetics, and equilibrium isotherm studies, the adsorption of methylene blue (MB) onto the synthesized SM-MAC is proposed to proceed via a synergistic, multi-stage mechanism, as illustrated in Figure 11. The overall adsorption process is not governed by a single type of interaction but rather results from the combined effects of efficient mass transfer, pore diffusion, and various physicochemical interactions occurring on the heterogeneous surface of the magnetic activated carbon nanocomposite.

In the initial stage, methylene blue molecules migrate from the solution toward the external surface of the adsorbent, driven by the concentration gradient between the solution and the adsorbent. During this phase, the large external surface area and interconnected pore entrances facilitate rapid adsorption; this accounts for the sharp increase in adsorption capacity observed during the early period of the process.

Subsequently, methylene blue molecules diffuse through the well-developed mesoporous network within the activated carbon matrix. An average pore diameter of approximately 2.77 nm, exceeding the effective molecular size of methylene blue (about 1.4 nm) [54], enables efficient intraparticle diffusion with minimal steric hindrance. This favorable pore architecture reduces diffusion resistance and promotes effective utilization of internal adsorption sites, thereby contributing to both high adsorption capacity and rapid adsorption kinetics.

Upon reaching the internal surface, methylene blue molecules are retained through several complementary interaction mechanisms. Graphitic domains within the activated carbon promote strong π–π interactions with the aromatic rings of the methylene blue. Simultaneously, hydroxyl and oxygen-containing functional groups identified via FTIR contribute to the formation of hydrogen bonds and dipole-dipole interactions, thereby enhancing the adsorbent's affinity for the dye molecules. Depending on solution chemistry, specifically the solution pH and the surface charge of the adsorbent, electrostatic attraction forces may also contribute to the adsorption process. The species with a negative charge, represented as $–COOH \rightarrow –COO^-$ [53], will attract positively charged species such as MB^+. However, additional surface charge characterization, such as zeta potential or pH_pzc measurements, is required to quantify the relative contribution of these electrostatic interactions. This step will be undertaken in future research.

The heterogeneous distribution of magnetic phases including Fe_3O_4, Fe_2O_3, Fe_3C, and metallic Fe

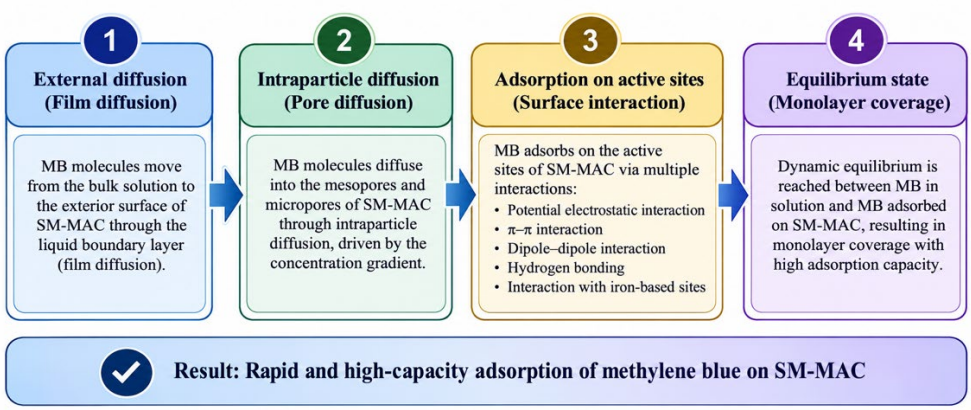

Figure 11: Schematic diagram of the proposed adsorption mechanism

further enhances the adsorption process by creating surface sites with varying adsorption energies. This structural heterogeneity expands the range of potential interactions between the adsorbate and the adsorbent, thereby increasing the likelihood of dye molecules being trapped within the porous carbon framework. While the primary function of the magnetic phases is to enable rapid magnetic separation following adsorption, they also contribute indirectly by improving nanoparticle dispersion and maintaining the composite's structural integrity.

Adsorption kinetics and equilibrium results further substantiate the proposed mechanism. The excellent fit with the pseudo-second-order model suggests that the adsorption rate is primarily governed by the progressive filling of surface-active sites, whereas the superior fit with the Langmuir isotherm indicates that monolayer adsorption is the dominant behavior within the studied concentration range. Nevertheless, given the multiphase composition and chemically heterogeneous surface of SM-MAC, these models should be interpreted as representations of dominant adsorption behavior rather than indications of an ideal homogeneous surface or a single adsorption pathway.

Overall, the adsorption of methylene blue onto SM-MAC is driven by a synergistic combination of rapid external mass transfer, efficient intraparticle diffusion through the mesoporous carbon network, π–π interactions, hydrogen bonding, dipole-dipole interactions, potential electrostatic attractions, and adsorption at heterogeneous active sites associated with the magnetic phases as depicted in Figure 11. The integration of these mechanisms accounts for the high adsorption capacity, rapid adsorption kinetics, excellent magnetic recovery, and good reusability of the synthesized SM-MAC, while highlighting its potential as an efficient and sustainable adsorbent for the treatment of dye-contaminated wastewater.

4 Conclusion

A superparamagnetic multiphase magnetic activated carbon (SM-MAC) nanocomposite was effectively synthesized using a straightforward low-oxygen method that does not require inert gas. The resultant material exhibited a high surface area, mesoporosity, and exceptional magnetic properties, which enable rapid adsorption and easy recovery. In this study, the adsorption isotherm of methylene blue conforms to the Langmuir model, while the kinetics of adsorption align with the pseudo-second-order model. With an adsorption capacity between 81 and 100 mg/g at pH levels ranging from 4.8 to 9.1 and excellent reusability, the SM-MAC shows potential for wastewater treatment applications, especially in the removal of methylene blue (MB). Although the proposed adsorption mechanism is well supported by structural characterization and adsorption behavior, further spectroscopic investigations (e.g., XPS, FTIR after adsorption, Raman spectroscopy, and zeta potential measurements) are recommended to provide direct evidence of the interactions between MB molecules and the SM-MAC surface.

Acknowledgements

The authors express their gratitude to Deputy of Research and Innovation Infrastructure of National Research and Innovation Agency (BRIN) for the assistance in sample characterization via ELSA.

Author contributions

A.H.: Writing – review & editing, Validation, Supervision, Formal analysis, Conceptualization. **D.G.S.:** Writing – review & editing, Writing – original draft, Validation, Supervision, Resources, Project administration, Funding acquisition, Investigation, Formal analysis, Conceptualization. **R**: Writing – review & editing, Validation, Resources, Formal analysis, Conceptualization. **H.W.**: Visualization, Validation, Resources, Methodology, Investigation, Formal analysis, Data curation.

Conflicts of Interest

The authors declare no conflict of interest.

Declaration of generative AI and AI-assisted technologies in the writing process

The authors utilized an online free paraphrasing-tool [https://ahrefs.com/writing-tools/paraphrasing-tool] and chatGPT to enhance the language and readability of the manuscript.

References

[1] N. Gupta, A. K. Kushwaha, and M.C. Chattopadhyaya, “Application of potato

(*Solanumtuberosum*) plant wastes for the removal of methylene blue and malachite green dye from aqueus solution," *Arabian Journal of Chemistry*, vol. 9, pp. S707-S716, 2016, doi:10.1016/j.arabjc.2011.07.021.

[2] N. A. Zainol et al., "Removal of methylene blue dye from aqueous solution by using orange peel treated with acid as an adsorbent," *Desalination and Water Treatment*, vol. 260, pp. 161–168, Jun. 2022, doi: 10.5004/dwt.2022.28425.

[3] R. Zein, J. S. Purnomo, P. Ramadhani, Safni, M. Fajri Alif, and C.N. Putri, "Enhancing sorption capacity of methylene blue dye using solid waste of lemon grass biosorbent by modification method," *Arabian Journal of Chemistry*, vol. 16, no. 10, Art. no. 104480, 2023, doi:10.1016/j.arabjc.2022.104480.

[4] E. Misran, W. P. M. D. Supardan, N. K. I. Kasyidi, D. A. Iryani, and V. Pramananda, "Ultrasonic-assisted adsorption of methylene blue using shrimp shells as a low-cost adsorbent: Evaluation on the adsorption isotherm, kinetics, and thermodynamics," *South African Journal of Chemical Engineering*, vol. 52, pp. 111–126, Apr. 2025, doi: 10.1016/j.sajce.2025.01.011.

[5] R. Ramadan and N. Shehata, "Adsorptive removal of methylene blue onto MFe2O4: Kinetics and isotherm modeling," *Desalination and Water Treatment*, vol. 227, pp. 370–383, Jul. 2021, doi: 10.5004/dwt. 2021.27248.

[6] Y. Luoyang et al., "Blue coke-based activated carbon adsorbents: Insights into the efficiency and mechanism of methyl blue removal," *Arabian Journal of Chemistry*, vol. 17, Art. no. 105898, Sep. 2024, doi: 10.1016/j.arabjc. 2024.105898.

[7] G. Liu, Y. Li, J. Hou, Y. Wang, and D. Lin, "A review on the industrial waste based adsorbents for the removal of pollutants from water: Modification methods and adsorption study," *Resources, Environment and Sustainability*, vol. 19, Art. no. 100183, Mar. 2025, doi: 10.1016/j.resenv.2024.100183.

[8] M. Ashrafi, M. Arab Chamjangali, G. Bagherian, N. Goudarzi, and S. Kavian, "Evaluation of nanosilica, extracted from stem sweep, as a new adsorbent for simultaneous removal of crystal violet and methylene blue from aqueous solutions," *Desalination and Water Treatment,* vol. 88, pp. 207–220, Sep. 2017, doi: 10.5004/dwt. 2017.21425.

[9] C. A. Mbachu, A. K. Babayemi, T. C. Egbosiuba, J. I. Ike, I. J. Ani, and S. Mustapha, "Green synthesis of iron oxide nanoparticles by Taguchi design of experiment method for effective adsorption of methylene blue and methyl orange from textile wastewater," *Results in Engineering*, vol. 19, Art. no. 101198, Sep. 2023, doi" 10.1016/j.rineng. 2023.101198.

[10] V. Kumaravelan and P. Sivakumar, "Fe_3O_4 immobilized magnetic nano carbon balls for the adsorption of methylene blue dye in batch and packed bed column mode," *Desalination and Water Treatment*, vol. 115, pp. 288–299, May 2018, doi: 10.5004/dwt.2018.22458.

[11] D. Joshy, P. J. Chamundi, N. K. Puthenveettil, Y. A. Ismail, and P. Periyat, "Mechanistic investigation of mesoporous Mg2+ doped CeO2 encapsulated Fe3O4 core-shells for the selective adsorptive removal of malachite green," *Results in Engineering*, vol. 20, Art. no. 101409, Dec. 2023, doi: 10.1016/j.rineng.2023.101409.

[12] M. S. Kothari et al., "Sustainable synthesis of carbide slag waste derived hydroxyapatite and its application for cationic dye adsorption," *Journal of Water Process Engineering*, vol. 66, Art. no. 106001, Sep. 2024, doi: 10.1016/j.jwpe.2024.10 6001.

[13] A. Tariq, N. Yahaya, and M. Sajid, "Low cost adsorbents derived from vegetables and fruits: Synthesis, properties, and applications in removal of heavy metals from water," *Desalination and Water Treatment*, vol. 320, Art. no. 100626, Oct. 2024, doi: 10.1016/j.dwt. 2024.100626.

[14] F. Sannino et al., "Two alternative approaches for the magnetic adsorption of the hydrophobic dye methylene blue," *Journal of Molecular Liquids*, vol. 409, Art. no. 125395, Sep. 2024, doi: 10.1016/j.molliq.2024.125395.

[15] K. Jedynak, M. Repelewicz, K. Kurdziel, and D. Wideł, "Mesoporous carbons as adsorbents to removal of methyl orange (anionic dye) and methylene blue (cationic dye) from aqueous solutions," *Desalination and Water Treatment*, vol. 220, pp. 363–379, Apr. 2021, doi: 10.5004/dwt.2021.26925.

[16] A. M. Zayed et al., "Facile synthesis of eco-friendly activated carbon from leaves of sugar beet waste as a superior nonconventional adsorbent for anionic and cationic dyes from aqueous solutions," *Arabian Journal of*

Chemistry, vol. 16, Art. no. 104900, Apr. 2023, doi:10.1016/j.arabjc.2023.104900.

[17] J. Sun, T. Xue, and J. Liu, "Biomass-derived porous carbon for rapid adsorption of methylene blue in aqueous solution," *Next Materials*, vol. 7, Art. no. 100452, Apr. 2025, doi: 10.1016/j.nxmate.2024.100452.

[18] F. Luziana, M. Rilyanti, and Sumadi, "Production of adsorbent from activated carbon of palm oil shells coated by Fe3O4 particle to remove crystal violet in water," *Desalination and Water Treatment*, vol. 171, pp. 281–293, Dec. 2019, doi: 10.5004/dwt.2019. 24776.

[19] S. Joshi, V. K. Garg, N. Kataria, and K. Kadirvelu, "Applications of Fe3O4@AC nanoparticles for dye removal from simulated wastewater," *Chemosphere*, vol. 236, Art. no. 124280, Dec. 2019, doi: 10.1016/j.chemosphere. 2019.07.011.

[20] N. E. Nkosi, P. M. Thabede, and N. D. Shooto, "One pot synthesis of Fe3O4-chili carbon composite removing methylene blue, paracetamol and nickel ions from an aqueous solution," *Case Studies in Chemical and Environmental Engineering*, vol. 10, Art. no. 100800, Dec. 2024, doi: 10.1016/j.cscee.2024.100800.

[21] S. Ali, Y. Abbas, Z. Zuhra, and I. S. Butler, "Synthesis of γ-alumina (Al2O3) nanoparticles and their potential for use as an adsorbent in the removal of methylene blue dye from industrial wastewater," *Nanoscale Advances*, vol. 1, no. 1, pp. 213–218, Jan. 2019, doi: 10.1039/c8na00014j.

[22] F. I. M. S. Sangor and M. A. Al-Ghouti, "Waste-to-value: Synthesis of nano-aluminum oxide (nano-γ-Al2O3) from waste aluminum foils for efficient adsorption of methylene blue dye," *Case Studies in Chemical and Environmental Engineering*, vol. 8, Art. no. 100394, Dec. 2023, doi: 10.1016/j.cscee.2023. 100394.

[23] S. F. Rafie, H. Sayahi, H. Abdollahi, and N. Abu-Zahra, "Hydrothermal synthesis of Fe3O4 nanoparticles at different pHs and its effect on discoloration of methylene blue: Evaluation of alternatives by TOPSIS method," *Materials Today Communications*, vol. 37, Art. no. 107589, Dec. 2023, doi: 10.1016/j.mtcomm.2023.107589.

[24] A. Ruíz-Baltazar, S. Y. Reyes-López, M. Mondragón-Sánchez, A. I. Robles-Cortés, and R. Pérez, "Eco-friendly synthesis of Fe3O4 nanoparticles: Evaluation of their catalytic activity in methylene blue degradation by kinetic adsorption models," *Results in Physics*, vol. 12, pp. 989–995, Mar. 2019, doi: 10.1016/j.rinp.2018.12.037.

[25] H. Bouyarmane, S. Saoiabi, A. Laghzizil, A. Saoiabi, A. Rami, and M. El Karbane, "Natural phosphate and its derivative porous hydroxyapatite for the removal of toxic organic chemicals," *Desalination and Water Treatment*, vol. 52, pp. 7265–7269, Nov. 2014, doi: 10.1080/19443994.2013.831797.

[26] Z. Alhalili, "Green synthesis of copper oxide nanoparticles CuO NPs from Eucalyptus globoulus leaf extract: Adsorption and design of experiments," *Arabian Journal of Chemistry*, vol. 15, no. 1, Art. no. 103739, Jan. 2022, doi: 10.1016/j.arabjc.2022.103739.

[27] A. Atri et al., "Removal of textile pollutants from aqueous medium using biosynthesized CuO nanoparticles: Theoretical comparative investigation via analytical model," *Heliyon*, vol. 10, Art. no. e26285, Mar. 2024, doi:10.1016/j.heliyon.2024.e26285.

[28] H. Tajizadegan et al., "Study of methyl orange adsorption properties on ZnO–Al2O3 nanocomposite adsorbent particles," *Desalination and Water Treatment*, vol. 57, pp. 12324–12334, Jun. 2016, doi: 10.1080/19443994.2015.1049558.

[29] A. Deb, M. Kanmani, A. Debnath, K. L. Bhowmik, and B. Saha, "Preparation and characterization of magnetic CaFe2O4 nanoparticles for efficient adsorption of toxic Congo Red dye from aqueous solution predictive modeling by artificial neural network," *Desalination and Water Treatment*, vol. 89, pp. 197–209, Sep. 2017, doi: 10.5004/dwt. 2017.21361.

[30] A. Zourou et al., "Graphene oxide-CuFe2O4 nanohybrid material as an adsorbent of Congo red dye," *Carbon Trends*, vol. 7, Art. no. 100147, Apr. 2022, doi: 10.1016/j.cartre. 2022.100147.

[31] R. Istratie, M. Stoia, C. Pacurariu, and C. Locovei, "Single and simultaneous adsorption of methyl orange and phenol onto magnetic iron oxide_carbon nanocomposites," *Arabian Journal of Chemistry*, vol. 12, no. 8, pp. 3704–3722, Jan. 2015, doi: 10.1016/j.arabjc. 2015.12.012.

[32] A. A. Burbano, G. Gasco, F. Horst, V. Lassalle, and A. Mendez, "Production, characteristics and use of magnetic biochar nanocomposites as sorbents," *Biomass and Bioenergy*, vol. 172, Art. no. 106772, May 2023, doi: 10.1016/j.biombioe. 2023.106772.

[33] C. Chen, Z. Li, and H. Hu, "Single-step synthesis of eucalyptus sawdust magnetic activated carbon and its adsorption behavior for methylene blue," *RSC Advances*, vol. 9, pp. 22248–22262, Jul. 2019, doi: 10.1039/c9ra03490k.

[34] C. Li, H. Liu, X. Jiang, G. I. N. Waterhouse, Z. Zhang, and L. Yua, "Hierarchical Fe3O4/C with a flower-like morphology: A highly efficient and reusable dye adsorbent," *Synthetic Metals*, vol. 246, pp. 45–56, Dec. 2018, doi: 10.1016/j.synthmet.2018.09.010.

[35] D. W. Cho, J. Lee, Y. S. Ok, E. E. Kwon, and H. Song, "Fabrication of a novel magnetic carbon nanocomposite adsorbent via pyrolysis of sugar," *Chemosphere*, vol. 163, pp. 305–312, Nov. 2016, doi: 10.1016/j.chemosphere.2016.08.025.

[36] N. M. Salatein, M. Shabaan, and I. S. Fahim, "Comparing low-cost activated carbon made from coffee waste and bagasse to remove heavy metals and methylene blue dye," *Results in Chemistry*, vol. 13, Art. no. 102020, Jan. 2025, doi:10.1016/j.rechem.2025.102020.

[37] Y. He et al., "Highly efficient removal of methyl blue from aqueous solution using a novel nitrogen-doped porous magnetic carbon," *Desalination and Water Treatment*, vol. 173, pp. 409–419, Jan. 2020, doi: 10.5004/dwt. 2020.24658.

[38] L. L. Zhi and M. A. A. Zaini, "One-step synthesis of magnetic activated carbons for methylene blue dye removal : Activation conditions and adsorption studies," *Desalination and Water Treatment*, vol. 198, pp. 434–444, Sep. 2020, doi: 10.5004/dwt.2020.26095.

[39] M. Wei, P. Zhang, B. Zhang, and L. Zhao, "Synthesis of Fe3O4/C composites derived from cornstalk by one-step hydrothermal method as a reusable adsorbent for dyes," *Inorganic Chemistry Communications*, vol. 143, Art. no. 109762, Sep. 2022, doi: 10.1016/j.inoche. 2022.109762.

[40] C. Liang et al., "In-situ magnetic activated carbon produced from sludge, straw and steel slag for the effective adsorption of methylene blue," *Desalination and Water Treatment*, vol. 302, pp. 210–223, Aug. 2023, doi: 10.5004/dwt.2023.29631.

[41] M. Liu, J. Dong, W. Wang, M. Yang, M. Gu, and Y. R. Han, "Study of methylene blue adsorption from solution by magnetic graphene oxide composites," *Desalination and Water Treatment*, vol. 147, pp. 398–408, Apr. 2019, doi: 10.5004/dwt.2019.23761.

[42] S. Fathi, R. R. Kalantary, A. Rashidi, and A. Karbassi, "Synthesis and characterization of magnetic nano-porous graphene functionalized with carboxyl for hexavalent chromium adsorption in aqueous solution," *Desalination and Water Treatment*, vol. 82, pp. 241–251, Jul. 2017, doi:10.5004/dwt.2017.20918.

[43] A. A. Aryee, R. Zhang, H. Liu, R. Han, Z. Li, and L. Qu, "Application of magnetic peanut husk for methylene blue adsorption in batch mode," *Desalination and Water Treatment*, vol. 194, pp. 269–279, Aug. 2020, doi: 10.5004/dwt. 2020.25862.

[44] N. Qin, C. Tian, L. Carter, D. Tao, Y. Zhou, and F. Zhang, "Economical magnetic activated carbon for methylene blue removal from water," *Next Sustainability*, vol. 4, Art. no. 100057, Jul. 2024, doi: 10.1016/j.nxsust.2024. 100057.

[45] W. Zhang, L. Y. Zhang, X. Zhao, and Z. Zhou, "Citrus pectin derived ultrasmall Fe3O4@C nanoparticles as a high-performance adsorbent toward removal of methylene blue," *Journal of Molecular Liquids*, vol. 222, pp. 995–1002, Oct. 2016, doi: 10.1016/j.molliq.2016. 07.144.

[46] D. Chen, J. Chen, Z. Hu, Y. Zhu, and H. Shen, "One-step synthesis of magnetic biosorbent for the removal of methylene blue," *Desalination and Water Treatment*, vol. 233, pp. 341–350, Sep. 2021, doi: 10.5004/dwt.2021.27523.

[47] N. B. Allou et al., "Methylene blue magnetic adsorption separation process from aqueous solution using corn cob," *Scientific African*, vol. 21, Art. no. e01828, Sep. 2023, doi: 10.1016/j.sciaf.2023.e01828.

[48] D. R. Vaddi, R. Malla, and S. Geddapu, "Magnetic activated carbon: A promising approach for the removal of methylene blue from wastewater," *Desalination and Water Treatment*, vol. 317, Art. no. 100146, Jan. 2024, doi: 10.1016/j.dwt.2024.100146.

[49] H. M. Ahmed, W. L. Kebede, A. B. Yaebyo, A. W. Digisu, and S. F. Tadesse, "Adsorptive removal of methylene blue dye by a ternary magnetic rGO/AK/Fe3O4 nanocomposite: Studying adsorption isotherms, kinetics, and thermodynamics," *Chemical Physics Impact*, vol. 10, Art. no. 100800, Jun. 2025, doi: 10.1016/j.chphi.2024.100800.

[50] C. Y. Yang, S. F. Hu, and C. L. Kao, "Fabrication of recyclable magnetic carbon material adsorbent from waste ion exchange resin," *Waste Management Bulletin*, vol. 1, pp. 205–216, Mar. 2024, doi: 10.1016/j.wmb.2023.10.005.

[51] C. G. Grigoras and A. I. Simion, "Synthesis of a new composite material derived from cherry stones and sodium alginate-application to the adsorption of methylene blue from aqueous solution: Process parameter optimization, kinetic study, equilibrium isotherms, and reusability," *Journal of Composites Science*, vol. 8, Art. no. 402, Oct. 2024, doi: 10.3390/jcs8100402.

[52] M. Husaini, Y. Danladi, and M. Hamza, "Regeneration and reusability of agricultural waste-derived adsorbent in the removal of cationic and anionic dyes," *Arabian Journal of Chemical and Environmental Research*, vol. 12, no. 2, pp. 152–166, 2025.

[53] L. Lelifajri, A. Hafizhah, K. Khirani, and A. A. Kacaribu, "NaOH-activated carbon from Gnetum gnemon L. shell waste for methylene blue adsorption from aqueous solutions," *Applied Science and Engineering Progress*, vol. 19, no. 4, Art. no. 8065, 2026, doi: 10.14416/j.asep. 2026.02.010.

[54] M. Chaharkam, M. Tahmasebpoor, and M. S. Yilmaz, "Exploring the structural characteristics and dye removal capabilities of powder-, granule- and film-shaped magnetic activated carbon derived from Oleaster seed," *Environmental Science and Pollution Research*, vol. 31, pp. 35283–35307, May 2024, doi : 10.1007/s11356-024-33598-y.